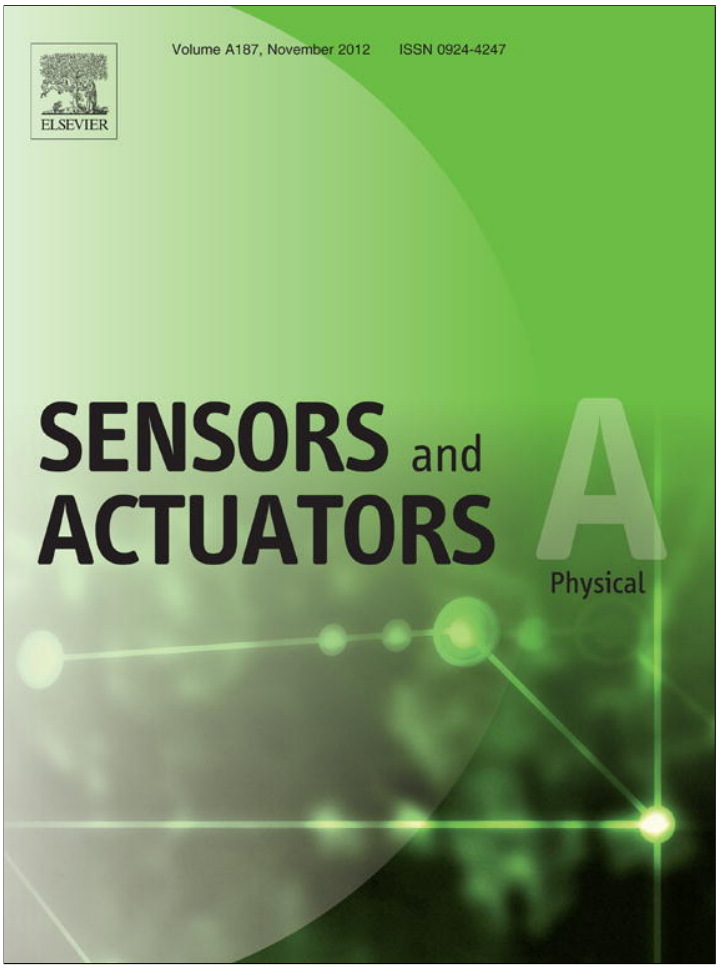

Sensors and Actuators A 187 (2012) 79–83

Contents lists available at SciVerse ScienceDirect

Sensors and Actuators A: Physical

journal homepage: www.elsevier.com/locate/sna

An overhanging carbon nanotube/parylene core–shell nanoprobe electrode

Takeshi Kawano[a,b,*], Chung Yeung Cho[a], Liwei Lin[a,**]

[a] Department of Mechanical Engineering and Berkeley Sensor and Actuator Center, University of California at Berkeley, Berkeley, CA 94720, USA
[b] Department of Electrical and Electronic Information Engineering, Toyohashi University of Technology, Toyohashi, Aichi 441-8580, Japan

ARTICLE INFO

Article history:
Received 27 January 2012
Received in revised form 29 July 2012
Accepted 15 August 2012
Available online 22 August 2012

Keywords:
Carbon nanotube
Assembly
Nanoprobe
Nanoelectrode
Intracellular electrode

ABSTRACT

A nanoprobe electrode based on electrically conductive carbon nanotube (CNT) as the core structure and biocompatible parylene-C as the insulating shell has been demonstrated. The prototype nanoprobe has been fabricated based on a local synthesis and assembly process using micromachined structures to synthesize suspended and both mechanically and electrically connected CNTs in a room temperature chamber. A 1.7-mm-long, overhanging silicon probe has been designed as the carrier for the CNT nanoprobe with typical length of a few micrometers. A conformal deposition of biocompatible parylene-C has been applied as the insulating layer and a local heating process at the distal end has been conducted to break and expose the CNT-tip section to open up the CNT core for possible electrical measurements. Experimental characterizations have shown good electrical interface between the base of the CNT and the growth-side microstructure, while the exposed CNT/parylene tip makes it attractive for applications in nano-scale electrical probing. These core–shell nanoprobe electrodes could find potential biomedical applications in intracellular electrical measurements.

1. Introduction

Micro-scale electrode arrays made by conventional microfabrication technologies have been applied in electrophysiological measurements of biological signals from cells or neurons [1–4]. It is desirable to construct nano-scale electrodes since microelectrodes are capable of measuring extracellular potential but difficult in retrieving intracellular signals due to the micro-scale electrode size. The typical magnitude of recorded extracellular signals is less than 100 μV, which is significantly lower than signals inside a cell of ~100 mV [5]. Other issues associated with micro electrodes are also in favor of nanoprobe developments, including: (1) large size of electrode may cause damage to tissues as well as cell membranes during experiments; (2) signal-to-noise ratio may be too low for meaningful intracellular detections; and (3) recorded signals could originate from several cells instead of a single living cell. These limiting factors might be addressed by next-generation cell recording devices using smaller electrodes such as nano-scale probes.

Previously, advancements in nanotechnology have demonstrated different fabrication processes for cylindrical bioprobe electrodes with diameters of less than 1 μm [6–8]. These and other nanobioprobes have enabled electrodes into cells for direct intracellular potential measurements [9] and DNA/biomolecules deliveries with sub-micro-scale spatial resolution [10]. A recent report has shown the feasibility for cellular probing applications by using a 100 nm in diameter carbon nanotube (CNT) and epoxy fixture for cellular studies [11]. CNT has been chosen in some of these previous studies due to its small diameter, mechanical robustness (large Young's modulus of 1.25 TPa for single walled CNT [12] and ~950 GPa for multiwalled CNT (MWCNT) [13], and high tensile strength [13]) and high electrical conductivity [14]. For the possible applications in electrical cellular probing, it is necessary to encapsulate the conductive-CNT with a biocompatible insulator and expose its tip for the electrical functionality [15]. Here we propose and demonstrate a process to construct such nanoprobe, based on the core–shell nanostructure of CNT/biocompatible parylene-C insulator.

2. Nanoprobe fabrication and assembly

We have demonstrated that suspended MWCNTs can be constructed by direct synthesis and assembly in localized chemical vapor deposition [16–18] and that the number of assembled CNTs can be controlled via real-time electrical feedback control [19,20]. We use this methodology to facilitate a nanobioprobe based on the CNT ("core"), which is subsequently encapsulated with a biological insulator ("shell"), followed by cutting the probe at the distal end to expose CNT-tip (Fig. 1a). Fig. 1(b)–(d) shows the schematic diagram of the fabrication process sequence. The MWCNT is grown

* Corresponding author at: 1-1 Hibarigaoka Tempaku-cho, Toyohashi, Aichi 441-8580, Japan. Tel.: +81 532 44 6738; fax: +81 532 44 6757.
** Corresponding author. Tel.: +1 510 643 5495; fax: +1 510 643 5599.
E-mail addresses: kawano@ee.tut.ac.jp (T. Kawano), lwlin@me.berkeley.edu (L. Lin).

0924-4247/$ – see front matter © 2012 Elsevier B.V. All rights reserved.
http://dx.doi.org/10.1016/j.sna.2012.08.025

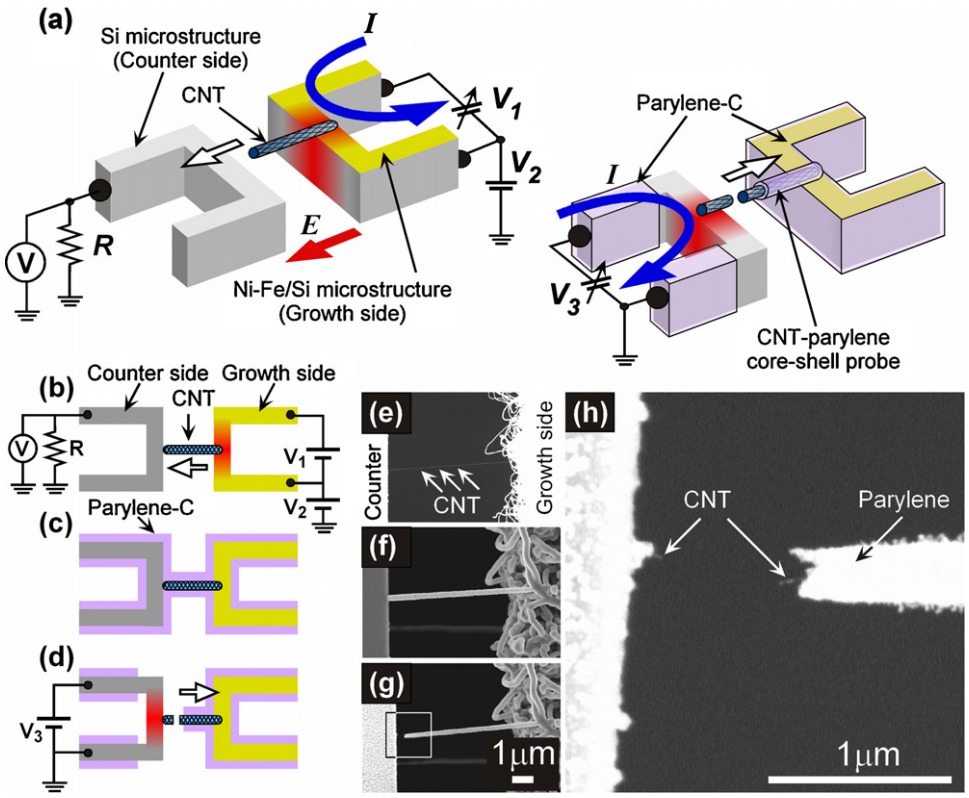

Fig. 1. Fabrication of an individual CNT/parylene core–shell nanoprobe electrode. (a) Schematically illustrated local CNT synthesis (left) and subsequent parylene-C encapsulation processes (right) using two silicon microstructures. (b) Schematic of the top-view of the CNT growth between two silicon structures by local (V_1) and electric-field-assisted (V_2) synthesis. The individual CNT is assembled via real-time electrical feedback control of the counter side (resistor, R and voltage meter, V), which configuration provides voltage signals when a CNT connection is made across the silicon structures. (c) Parylene-C deposition. (d) The simultaneous parylene removal from the CNT-tip and the CNT detachment by heating (V_3) the counter side silicon structure. (e) SEM image of as-grown single CNT between silicon structures (illustrated in schematic (b)), (f) parylene deposition around the CNT (schematic (c)), (g) the tip area exposed by heating of the counter side structure (schematic (d)), and (h) close-up-view of the exposed tip in image (g).

by the local synthesis process from the highly doped p-type silicon growth structure (resistivity of 1×10^{-2} Ωcm), which is coated with a 5-nm-thick nickel (Ni)–iron (Fe) layer as the catalyst. The process requires only a one mask process on a silicon-on-insulator (SOI) wafer. The shape of the microstructures (typically heaters with two contact areas) is defined by photolithography and etched by deep reactive-ion etching (DRIE). The oxide layer underneath the heaters is then removed in a time etching process which will preserve the oxide underneath the contact pad areas. The typical size of the silicon growth structure is 150 μm in length, 5 μm in width and 15 μm in thickness. With the applied voltage V_1 at about 7.5 V, the silicon structure is heated up by Joule heating (850–900 °C) [21]. A voltage V_2 of about 5 V is used for the local electric-field-assisted growth by providing a local electrical field to guide the growth of CNTs, achieving the self-assembly of a CNT between the two silicon structures (Fig. 1b) [19,20]. The synthesis is conducted in a room temperature vacuum chamber of 40 kPa with acetylene (C_2H_2) gas of 50 SCCM (SCCM denotes cubic centimeter per minute at STP). The number of CNTs getting synthesized and assembled across the two microstructures can be monitored and controlled by the electrical signals from the counter side electrode as shown in Fig. 1(b). During the CNT synthesis, once CNTs are made across the silicon microstructures, there are corresponding voltage jumps. By the number of voltage increases, we can determine the number of CNT connections [19,20]; here only one CNT can be assembled by stopping the heater after the first signal detected on the voltmeter V. The sidewall of the assembled CNT should entirely be covered with a good insulating thin layer, in order for potential biological applications including intracellular electrical measurements. Parylene-C is chosen as the insulator and applied in Fig. 1(c), because of its high electrical resistivity (~10^{16} Ωcm), biocompatibility with tissue and the capability of a highly conformal deposition at room temperature [22]. Finally, the parylene at the CNT-tip region is removed by heating the counter side silicon structure by applying the voltage V_3 of about 7.5 V at the counter electrode side as shown in Fig. 1(d), resulting in the evaporation of the parylene to expose the CNT-tip. This also causes the CNT to brake and detach from the silicon counter side due to the thermal contraction of the parylene around the CNT.

3. Experimental results and discussion

3.1. Assembled and tip exposed nanoprobe

Fig. 1(e)–(g) shows scanning electron microscope (SEM) images following the process sequence of Fig. 1(b)–(d) for building a CNT-based nanoprobe of about 7 μm in length as controlled by the gap distance between the two microstructures. Fig. 1(e) is an as-grown bridging CNT between the silicon structures (see Fig. 1b). Fig. 1(f) shows the fabrication result after the parylene deposition as all CNTs are uniformly encapsulated with parylene. Fig. 1(g) illustrates the exposed CNT-tip after heating the counter side silicon structure. It is believed that the detachment of the CNT from the counter side silicon structure is caused by the thermal contraction of the parylene which results in the melting and retraction of the parylene at the distal end of the CNT/parylene nanoprobe. Experimentally, the counter side silicon structure was heated for about 30 min, resulting in exposed CNT tip of about 100 nm in length, as shown in

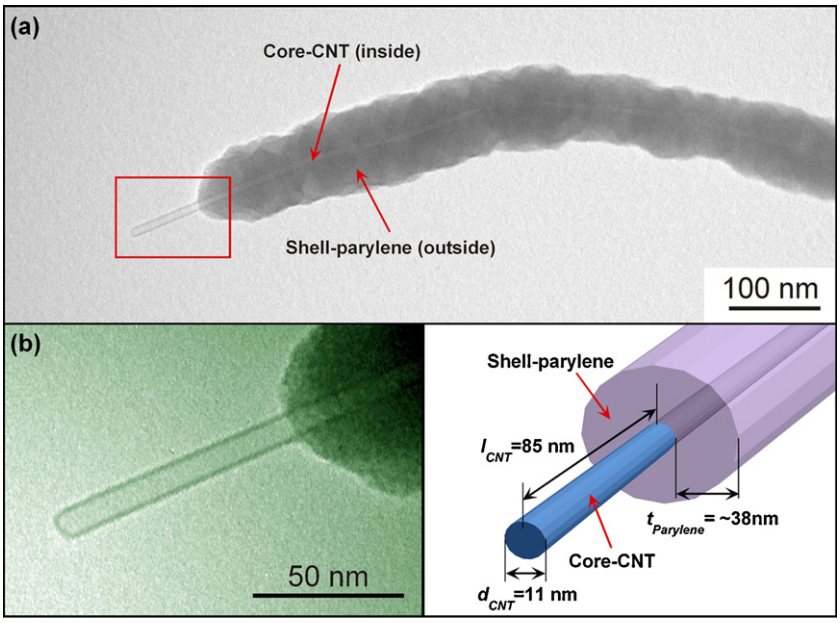

Fig. 2. A tip-exposed CNT/parylene core–shell nanoprobe. (a) TEM image shows core-CNT and shell-parylene. The diameter of the CNT, d_{CNT}, is 11 nm, and the thickness of the parylene, $t_{parylene}$, is 38 ± 6 nm. (b) Close-up-view (left) of the tip section of the probe in image (a) and schematic (right) of the probe-tip section. The length of the exposed CNT portion, l_{CNT}, is 85 nm.

Fig. 1(h). The deposition thickness of parylene can be controlled by the amounts of the parylene dimer used in the process and about 300 nm is the measured diameter for the sample in Fig. 1(h).

Fig. 2(a) shows the transmission electron microscope (TEM) image of the tip region of fabricated CNT/parylene nanoprobe. The diameter of the core-CNT, d_{CNT}, and the thickness of the shell-parylene, $t_{parylene}$, are 11 nm and 38 ± 6 nm, respectively, and the length of the exposed CNT portion, l_{CNT}, is 85 nm. Fig. 2(b) is the close up TEM image (left) of the exposed CNT section and the schematic diagram (right) illustrates the details around the tip-section. In general, the typical diameter of the CNT made by the local synthesis technology is between 10 and 50 nm and the length of the CNT can be designed by the opening gap between the two silicon structures which is between 5 and 25 μm in the prototype devices. The thickness of the parylene layer surrounding the core-CNT is between 30 and 150 nm as controlled by the amounts of the parylene dimer (0.05–0.1 g) in the depositing process. Although the constant heating voltage of V_3 = ~7.5 V for 30 min is used for the parylene removal from the CNT-tip and the CNT detachment, the length controllability of the exposed CNT tip from the parylene can be discussed using varied heating parameters of the temperature (room temperature to 950 °C [19]) and the time. A physical stretching method using two silicon microstructures is another considerable way to expose the core-CNT from the shell-parylene [23].

3.2. Electrical tests

MWCNTs grown by the local synthesis methodology exhibited metallic behavior with highly conductive characteristics [19,20]. The electrical connections of the single CNT to the two connecting microstructures (p-type silicon and each microstructures has resistance of 380 Ω) were electrically tested to confirm mechanical connection in the current I–voltage V measurements prior to the parylene deposition. I–V characteristics of the assembled CNT were measured after the synthesis process in an argon environment under the pressure of 9.82×10^3 Pa, by applying input voltages via the microstructures. To prevent the Joule heating of the CNT [20,24], the I–V curves were taken at low input voltage range of

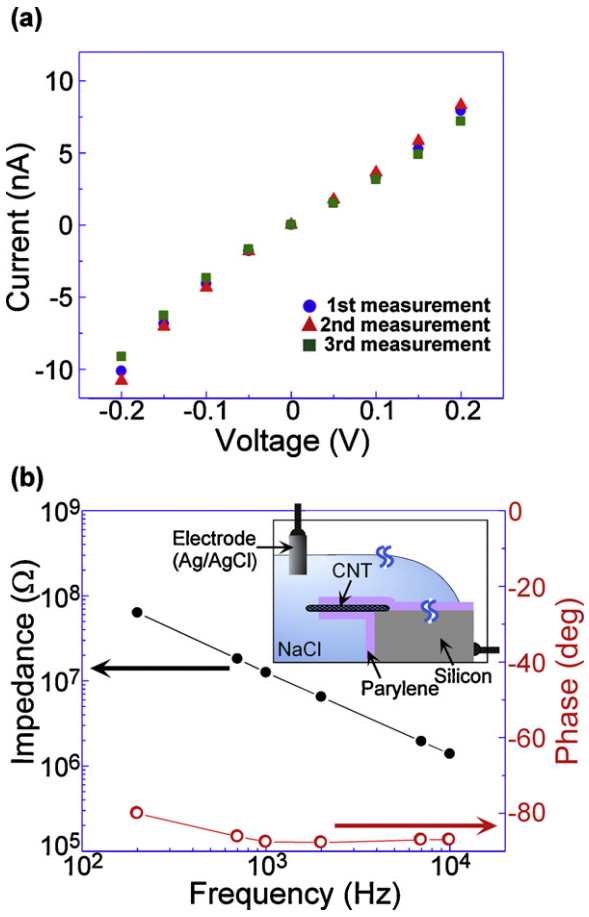

Fig. 3. Electrical testing on nanoprobe. (a) Electrical properties of a single core-CNT prior to the parylene deposition. Current I and voltage V curves were taken from a 22-μm-length bridging CNT with the diameter of about 30 nm. (b) Electrical impedance characteristics of a tip-exposed CNT/parylene core–shell probe electrode with the silicon microstructure. We used the same probe device shown in Fig. 1(h) for the measurement. Both the impedance magnitude and the phase angle of the nanoprobe device were taken in saline solution (0.9 wt.% sodium chloride, room temperature), using input sine waves with a amplitude of 10 mV_{pp}, 200 Hz–10 kHz.

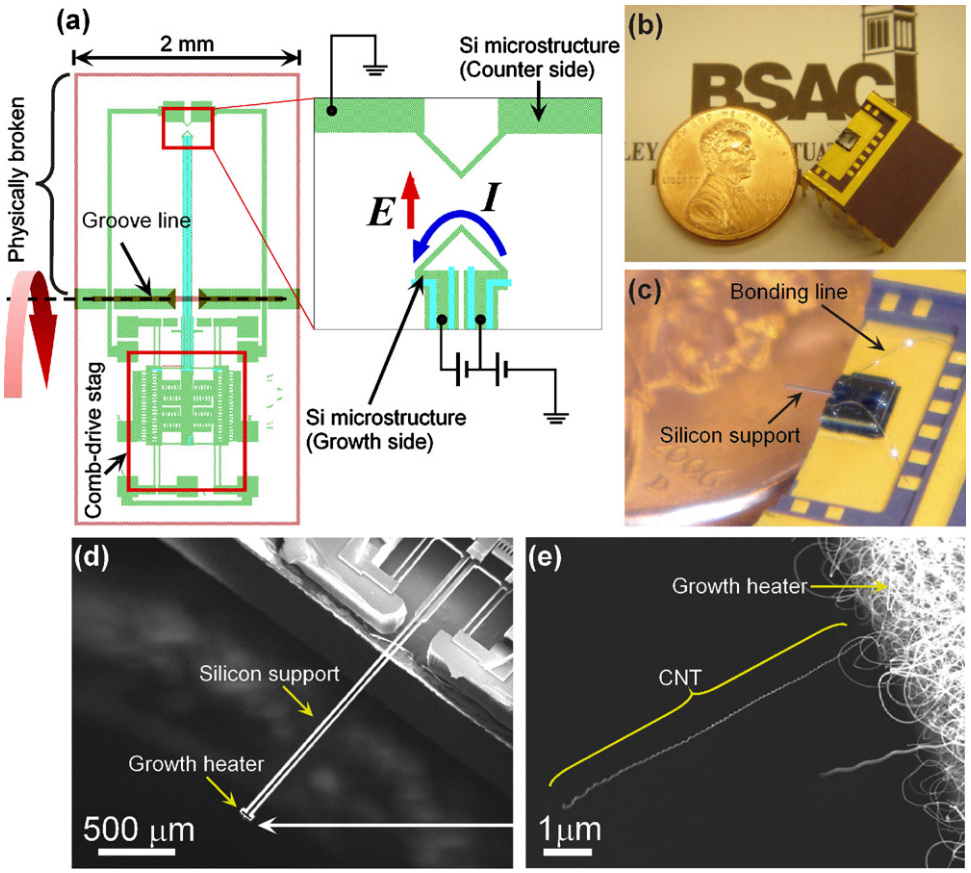

Fig. 4. Device packaging technique for nanoprobe using protruding silicon support. (a) Device layout for the protruding silicon support. The silicon growth heater is located at the tip of the support, while a *X*–*Y* comb-drive actuators provide more accurate positioning during the cellular probing. Photographs showing the device packaging and U.S. one cent (b), and close-up view (c) of the photograph image (b). (d) SEM image of the silicon support and the heater structure for the growth of CNT. (d) SEM image of a single CNT grown from the heater structure.

±200 mV. Fig. 3(a) shows typical *I*–*V* curves taken from a 22-μm-long bridging CNT with the diameter of about 30 nm. Repeated *I*–*V* measurements with resistance of 18.5–27.8 MΩ at ±200 mV, give a CNT resistance per micron length of 0.84–1.26 MΩ/μm. None of the state-of-art technologies can construct CNTs with controllable resistance and neither is the local synthesis of CNTs to provide the resistance control for assembled CNTs. This is due to uncontrollable CNT properties such as CNT diameter, chirality and defects in CNT. Our previous reports show that MWCNTs with diameters of 30–50 nm have exhibited varied resistances per micron length of 5.5 kΩ/μm–0.5 MΩ/μm at ±200 mV [19,20]. Due to the length dependent CNT resistance, a nanoprobe electrode with lower resistance requires a shorter CNT, which could be controlled by the gap between the silicon microstructures.

After confirming the electrical/mechanical connection, the parylene deposition process was conducted and the local heating process was performed to complete the fabrication process. Afterwards, the sample was wire-bonded for impedance characterizations. The impedance characteristics of a typical tip-exposed CNT/parylene nanoprobe in an electrolyte were measured using the same sample shown in Fig. 1(h). Herein we used saline solution (0.9 wt% sodium chloride, room temperature) as the electrolyte, and a test signal in sine waves with an amplitude 10 mV_{pp} at frequency range of 200 Hz–10 kHz was applied to the electrolyte through a silver/silver chloride counter electrode. Fig. 3(b) shows the impedance and phase angle taken from the nanoprobe device dipped in the electrolyte, with schematic diagram shown in the inset image. Because the nanoprobe device with the parylene/silicon-microstructure was immersed in the electrolyte, the measured impedances of 12.6–1.4 MΩ at 1–10 kHz were mainly dominated by the parasitic capacitance of the electrolyte/parylene/silicon-microstructure system, as confirmed by the measured phase angles of −87.5 to −86.9°. Smaller capacitor contributions to the measured impedance magnitude with the phase angles of −80° and −86.1° were observed at lower frequency of 200 Hz and 700 Hz, respectively, indicating that the CNT-tip/electrolyte interface-induced resistive impedance also contributed to the impedances of 63.3 MΩ and 18.2 MΩ. These measured impedances and phase angles were limited by the impedance range of our impedance analyzer while further characterizations could be obtained with more sophisticated measurement instruments and designs. For example, possible on-chip integration of electronic circuitry and better shielding materials could further reduce the background noise for stronger signals.

4. Nanoprobe packaging

The fabricated nanoprobe device also requires specific packaging techniques in applications such as cellular probing. For this particular experimental procedure, we have designed the elongated, overhanging silicon support with the growth heater structure positioned at its tip (Fig. 4a). Similar to the nanoprobe assembly techniques (Fig. 1), the counter side silicon structure is designed to assist the local electric-field-assisted growth of CNTs and the electrical heating for cutting of the CNT-tip. Furthermore, an extra micromachining step is added to the original SOI process with one more mask to define through-wafer openings from the backside of the wafer by using the DRIE process. These openings

serve as two purposes: (1) they allow direct observations under TEM to characterize the nanoprobe as electron can go through the substrate for analyses; (2) they provide packaging cut-off lines for easy breakage of individual devices. For example, a groove can be designed such that half of the substrate from the device unit can be physically broken along this pre-designated groove line, exposing the protruding silicon support as shown in Fig. 4(a).

Fig. 4(b) and (c) shows photographs of the device. In Fig. 4(b), the nanoprobe device is mounted on a conventional IC-package, which is cut with a diamond saw, and compared with a US one cent coin. In Fig. 4(c), the wire-bonds and the long silicon support probe structure can be observed. Typically, the length of the protruding silicon probe from the edge of the package results is 1.7 mm. Contacts on the device chip and the IC-package are electrically connected via aluminum bonding wires. Fig. 4(d) and (e) shows SEM images of the overhanging silicon support and the CNTs grown at the growth heater structure (located at the tip of the support). The design of the protruding silicon probe will allow the CNT probe to accurately access the targeted cells. Although we did not form the parylene shell for the CNT device (Fig. 4), the same process shown in Fig. 1(c) can be used to achieve the CNT/parylene nanoprobe, that is followed by the exposing of the CNT-tip from the shell-parylene by heating the designed counter side silicon structure. In the cell tests, the target cells can be placed in front of the CNT-based nanoprobe with in situ observation under a microscope. As preliminarily cell tests, cells on a substrate such as cultured cells can be used. Herein the CNT-based nanoprobe device is mounted on a standard *X–Y–Z* manipulation system to control placement positions of the CNT tip in the cell probing. The combination of the built-in micro actuator based on the silicon comb-drive stage could facilitate greater control for the placement position of the CNT tip.

5. Conclusion

We have described techniques for fabrication of the CNT/parylene core–shell nanoprobe electrode for potential biological applications. Using the growth heater and the counter side silicon microstructures, a single CNT can be locally grown and connected between the two structures as the core for the nanoprobe. The advantage of this fabrication process is that the length of the CNT, which is an important characteristic of the electrode, can be controlled by the predetermined gap width between the two silicon structures. The use of parylene-C as the insulating shell also promises biocompatible and conformal deposition around the CNT for insulating purposes. Finally, the parylene at the CNT tip can be removed selectively by heating up the counter silicon structure. The present work has proven the feasibility of making nanoprobes based on CNT/parylene core–shell nanostructures which might offer significant improvement over other intracellular probes due to the high conductivity, mechanical robustness, and extremely small feature size of the core CNT electrode.

Acknowledgments

Authors would like to thank Brian Sosnowchik for creating our data-collection software, as well as staff at the EML (Electron Microscopy Laboratory) at UC Berkeley, for their TEM work, and staff of the Berkeley Microfabrication Laboratory. T.K. is funded by the JSPS Postdoctoral Fellowships for Research Abroad from Japan.

References

[1] K.E. Jones, P.K. Compbell, R.A. Normann, A glass/silicon composite intracortical electrode array, Annals of Biomedical Engineering 20 (1992) 423–437.
[2] K. Najafi, K.D. Wise, T. Mochizuki, A high-yield IC-compatible multichannel recording array, IEEE Transactions on Electron Devices ED-32 (1985) 1206–1211.
[3] J.P. Donoghue, Connecting cortex to machines: recent advances in brain interfaces, Nature Neuroscience 5 (2002) 1085–1088.
[4] L.R. Hochberg, M.D. Serruya, G.M. Friehs, J.A. Mukand, M. Saleh, A.H. Caplan, A. Branner, D. Chen, R.D. Penn, J.P. Donoghue, Neuronal ensemble control of prosthetic devices by a human with tetraplegia, Nature 442 (2006) 164–171.
[5] J.G. Nicholls, A.R. Martin, B.G. Wallace, P.A. Fuchs, From Neuron to Brain, 4th ed., Sinauer Associates, Inc., Massachusetts, 2001.
[6] I. Obataya, C. Nakamura, S. Han, N. Nakamura, J. Miyake, Nanoscale operation of a living cell using an atomic force microscope with a nanoneedle, Nano Letters 5 (2005) 27–30.
[7] S. Nagasawa, H. Arai, R. Kanzaki, I. Shimoyama, Integrated multi-functional probe for active measurements in a single neural cell, in: Proceedings Transducers, 2005, 2005, pp. 1230–1233.
[8] N.A. Kouklin, W.E. Kim, A.D. Lazareck, J.M. Xu, Carbon nanotube probes for single-cell experimentation and assays, Applied Physics Letters 87 (2005) 173901.
[9] B. Tian, T. Cohen-Karni, Q. Qing, X. Duan, P. Xie, C.M. Lieber, Three-dimensional flexible nanoscale field-effect transistors as localized bioprobes, Science 329 (2010) 830–834.
[10] X. Chen, A. Kis, A. Zettl, C.R. Bertozzi, A cell nanoinjector based on carbon nanotubes, Proceedings of the National Academy of Sciences of the United States of America 104 (2007) 8218–8222.
[11] R. Singhal, Z. Orynbayeva, R.V.K. Sundaram, J.J. Niu, S. Bhattacharyya, E.A. Vitol, M.G. Schrlau, E.S. Papazoglou, G. Friedman, Y. Gogotsi, Multifunctional carbon-nanotube cellular endoscopes, Nature Nanotechnology 6 (2011) 57–64.
[12] A. Krishnan, E. Dujardin, T.W. Ebbesen, P.N. Yianilos, M.M.J. Treacy, Young's modulus of single-walled nanotubes, Physical Review B 58 (1998) 14013–14019.
[13] M.F. Yu, O. Lourie, M.J. Dyer, K. Moloni, T.F. Kelly, R.S. Ruoff, Strength and breaking mechanism of multiwalled carbon nanotubes under tensile load, Science 287 (2000) 637–640.
[14] T.W. Ebbesen, H.J. Lezec, H. Hiura, J.W. Bennett, H.F. Ghaemi, T. Thio, Electrical conductivity of individual carbon nanotubes, Nature 382 (1996) 54–56.
[15] T. Kawano, C.Y. Cho, L. Lin, Carbon nanotube-based nanoprobe electrode, in: Proceedings of the IEEE Nano/Micro Engineering and Molecular Systems Conference (NEMS), Bangkok, Thailand, 16–19 January, 2007, pp. 895–898.
[16] O. Englander, D. Christensen, L. Lin, Local synthesis of silicon nanowires and carbon nanotubes on microbridges, Applied Physics Letters 82 (2003) 4797–4799.
[17] O. Englander, D. Christensen, J. Kim, L. Lin, S. Morris, Electric-field assisted growth and self-assembly of intrinsic silicon, Nano Letters 5 (2005) 705–708.
[18] Q. Zhou, L. Lin, Enhancing mass transport for synthesizing single-walled carbon nanotubes via microchemical vapor deposition, Journal of Microelectromechanical Systems 20 (2011) 9–11.
[19] T. Kawano, D. Christensen, S. Chen, C.Y. Cho, L. Lin, Formation and characterizations of silicon/carbon nanotube/silicon heterojunctions by local synthesis and assembly, Applied Physics Letters 89 (2006) 163510.
[20] T. Kawano, H. Chiamori, M. Suter, Z. Qin, B. Sosnowchik, L. Lin, An electrothermal carbon nanotube gas sensor, Nano Letters 7 (2007) 3686–3690.
[21] L. Lin, M. Chiao, Electrothermal responses of lineshape microstructures, Sensors and Actuators A A55 (1996) 35–41.
[22] G.E. Loeb, M.J. Bak, M. Salcman, E.M. Schmidt, Parylene as a chronically stable reproducible microelectrode insulator, IEEE Transactions on Biomedical Engineering BME 24 (1977) 121–128.
[23] Y. Takei, T. Kan, K. Matsumoto, I. Shimoyama, Nanoprobe electrodes cut by physical stretch of parylene-insulated carbon nanotube bridges, in: Proceedings of the International Solid-State Sensors, Actuators and Microsystems Conference (TRANSDUCERS), Beijing, China, 5–9 June, 2011, pp. 2586–2589.
[24] K. Mølhave, S.B. Gudnason, A.T. Pedersen, C.H. Clausen, A. Horsewell, P. Bøggild, Transmission electron microscopy study of individual carbon nanotube breakdown caused by joule heating in air, Nano Letters 6 (2006) 1663–1668.